Measurement of the field-induced dielectronic-recombination-rate enhancement of O^{5+} ions differential in the Rydberg quantum number n

S. Böhm,*,† S. Schippers,† W. Shi,† and A. Müller†
Institut für Kernphysik, Universität Giessen, 35392 Giessen, Germany

N. Eklöw and R. Schuch
Atomic Physics, Stockholm University, 10405 Stockholm, Sweden

H. Danared
Manne Siegbahn Laboratory, 10405 Stockholm, Sweden

N. R. Badnell
Department of Physics and Applied Physics, University of Strathclyde, Glasgow G4 0NG, United Kingdom

D. M. Mitnik and D. C. Griffin
Department of Physics, Rollins College, Winter Park, Florida 32789
(Received 15 January 2002; published 14 May 2002)

The influence of electromagnetic fields on the dielectronic recombination of O^{5+} ions has been measured at the Stockholm heavy ion storage ring CRYRING. The experimental energy range covered all $2s \rightarrow 2p$ $\Delta n = 0$ resonances. Electric fields up to 600 V/cm were applied and a noticeable enhancement of the dielectronic recombination cross section as a function of electric-field strength was observed. Field ionization of highly exited Rydberg states was used to investigate the enhancement of the recombination rate for two narrow bands of n states ranging from $n \approx 19$–22 and from $n \approx 23$–25. The experimental data are compared to theory. After applying a field-ionization model to the calculations, the field-free spectra show good agreement with the experimental data. Although experiment and theory show the same trend of increasing strength of dielectronic recombination with increasing external electric field and with increasing n, quantitative discrepancies remain.

DOI: 10.1103/PhysRevA.65.052728 PACS number(s): 34.80.Lx

I. INTRODUCTION

Dielectronic recombination (DR) of an ion and an electron is a resonant two-step process in which the dielectronic capture of the projectile electron into a doubly excited intermediate state $|d\rangle$ is followed by the radiative decay of this state to a bound level below the first ionization limit. The doubly exited state can be weakly bound and hence be very sensitive to the influence of electromagnetic fields. Dielectronic recombination in the presence of external electromagnetic fields (DRF) was studied first theoretically by Burgess and Summers [1] and Jacobs *et al.* [2,3]. It was recognized that an external electric field mixes states with different orbital quantum numbers, which leads to an enhancement of the DR cross section. Discrepancies between theory and experiment in early DR measurements were speculatively ascribed to the existence of electric fields in the interaction region and stimulated further theoretical investigations.

The first DRF experiment was carried out by Müller *et al.* with a crossed beams apparatus using sodiumlike Mg^+ ions [4,5]. Differences from theoretical results [6,7] were in the order of 15–25%. DRF measurements with highly charged ions became feasible with the implementation of the merged-beams method at heavy-ion storage rings. The first such experiment was carried out by Bartsch *et al.* [8] with lithiumlike Si^{11+} ions at CRYRING at the Manne Siegbahn Laboratory in Stockholm. Lithiumlike ions have been chosen for this and the following experiments because of their favorable q/m ratio that requires minimum magnetic fields in the bending magnets of a storage ring. In comparison with other isoelectronic sequences this leads to the least effect of field ionization of Rydberg states produced by the recombination processes. Lithiumlike ions are also favorable because of their fairly simple electronic structure.

As the electric field imposed on the interaction region of Si^{11+} ions and electrons was increased the recombination rate of the high Rydberg states increased up to a factor of 2.5. Comparison of experiment and theory showed qualitative agreement. It was speculated that the remaining discrepancies might possibly be ascribed to the magnetic field $B_\parallel$ that guides the electron beam through the cooling device. This magnetic field that is perpendicular to the applied electric field had not been considered in the theoretical analysis of the Si^{11+} DRF experiment of Bartsch *et al.* [8]. In a theoretical model investigation Robicheaux and Pindzola [9] qualitatively showed that a magnetic field perpendicular to the applied electric field influences the recombination rate by additional magnetic sublevel mixing. This was verified with an experiment on Cl^{14+} at the heavy-ion storage ring TSR of the Max-Planck Institute for Nuclear Physics in Heidelberg [10]. The magnetic field perpendicular to the electric field was varied, and indeed an effect on the recombination rate

*Email address: Sebastian.G.Boehm@physik.uni-giessen.de
†Electronic address: http://www.strz.uni-giessen.de/~k3

was observed. However, due to the complexity of the problem, no theory was available to which these data could be compared quantitatively.

The difficulties enter via the influence of the magnetic field on the magnetic sublevel population. As long as only electric fields are present the magnetic quantum number m remains a good quantum number. This is still valid if a magnetic field parallel to the electric field exists, which was verified experimentally by Klimenko *et al.* [11]. Applying an additional perpendicular magnetic field breaks the cylindrical symmetry and an explicit treatment of each m substate is required in the diagonalization of the Hamiltonian. Presently such calculations can only be carried out for low values of n ($n<30$), since the size of the matrices to be diagonalized increases as n^2. An example for such a calculation is given in Ref. [12] for the $n=24$ resonance of Si^{11+}. Unfortunately, such Rydberg resonances cannot be resolved in the experiments. The measured enhancement can only be observed as an average value for the sum of states influenced by electromagnetic fields to which a detailed comparison with theory is hardly possible.

To minimize the number of states that have to be considered in the theoretical treatment, we here introduce a differential field-ionization technique for the storage ring measurements; it is similar to the one that was used previously for measuring DRF of a narrow band of Rydberg states in Mg^+ [4,5]. This method utilizes state selective field ionization of Rydberg states. The present experiment also extends a series of measurements on lithium-like ions (Ne^{7+} [13], Si^{11+} [8], Cl^{14+} [10], Ti^{19+} [14], and Ni^{25+} [15]) towards lower values of the nuclear charge number Z.

In Sec. II an outline of DRF is given. Some general remarks on the theory that is compared to the experiment are given in Sec. III. Sec. IV describes the experimental procedure with special emphasis on field ionization. The results are presented in Sec. V and compared to theoretical calculations. We summarize the paper in Sec. VI.

II. MODEL DESCRIPTION OF DRF

For the present case, DR can be represented by

$$e^- + O^{5+}(1s^2 2s) \rightarrow O^{4+}(1s^2 2pnl) \rightarrow \begin{cases} O^{4+}(1s^2 2s\ nl) + h\nu & \text{(type I)} \\ O^{4+}(1s^2 2pn'l') + h\nu' & \text{(type II)}. \end{cases} \tag{1}$$

Type II transitions involve the radiative decay of the Rydberg electron. Because of the rapid decrease of radiative rates with increasing n, type II transitions are unimportant for high-n states and are therefore neglected in the following discussion of DRF via high-n Rydberg states. The lowest Rydberg state that is energetically allowed is $n=6$. The position of the resonances can be represented by

$$E_n = E_{2s\rightarrow 2p} - \mathcal{R}\left(\frac{q}{n}\right)^2, \tag{2}$$

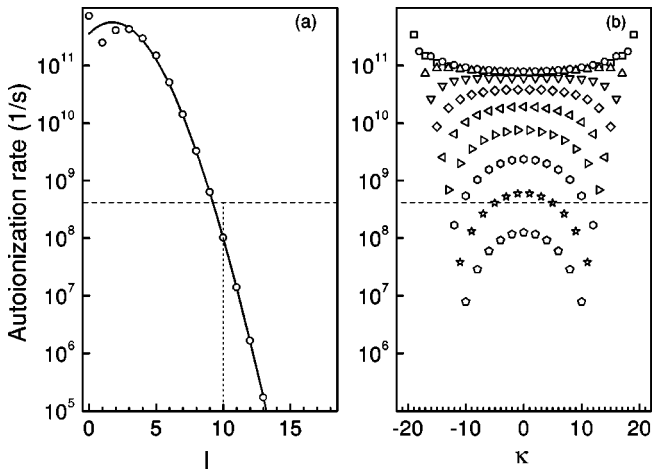

FIG. 1. (a) Configuration-averaged autoionization rates of $O^{4+}(1s^2 2p 20l)$ states calculated by AUTOSTRUCTURE (open circles). The full curve was obtained by fitting Eq. (4) to the data points with the fit parameters $\tilde{A}_a = 3.535\times 10^{11}\ s^{-1}$, $\tilde{d}_1 = 0.5424$, $\tilde{d}_2 = -0.1633$, $\tilde{d}_3 = 0.002\,740$, and $\tilde{d}_4 = 0$. The horizontal dashed lines represents the radiative rate of the $2p\rightarrow 2s$ transition and the vertical line the value of the critical angular-momentum quantum number l_c. (b) Configuration-averaged autoionization rates $A_a(n,\kappa,m)$ of $O^{4+}(1s^2 2p\ 20\kappa m)$ states as given by Eq. (8). The m-substates $|m|=0$ to $|m|=9$ are denoted by the following symbols beginning with $|m|=0$: squares, circles, up triangles, inverted triangles, diamonds, left triangles, right triangles, hexagons, stars, and pentagons. The number of states participating in DR is 1200 in (a) and 1608 in (b), i.e., the states with $A_a > A_r$.

where $E_{2s\rightarrow 2p}$ is the energy of the $2s$ to $2p$ transitions shown in Eq. (1), $\mathcal{R}$ is the Rydberg constant, and q is the charge of the ion in units of the elementary charge. The cross section for DR is given by the product of the cross section for the dielectronic capture σ_c and the branching ratio for stabilization $[A_r/(A_r+A_a)]$, where A_r and A_a are the radiative and autoionization rates, respectively, of the intermediate resonant state $|d\rangle$ with configuration $2pnl$. Dielectronic capture is the inverse of autoionization. From the principle of detailed balance, it follows $\sigma_c = kA_a$, where k includes statistical factors. The DR resonance strength (integrated cross section) can then approximately be represented by

$$\overline{\sigma}_{nl}^{(\mathrm{DR})} = S_0 \frac{g_d}{g_i}\frac{\pi}{E_n}\left[\frac{A_a(n,l)A_r}{A_a(n,l)+A_r}\right]. \tag{3}$$

The quantities $g_d = 12(2l+1)$ and $g_i = 2$ are the statistical weights of the intermediate $1s^2 2pnl$ and initial $1s^2 2s$ state, respectively, E_n is the resonance energy and S_0 is a constant ($S_0 \approx 10^{-29}\ \mathrm{cm^2\,eV^2\,s}$).

The autoionization rates A_a strongly depend on the quantum numbers n and l. They are large for small values of n and l and decrease with n as n^{-3}. They decrease even more rapidly with increasing l, since the overlap of the wave functions of the inner and outer electron decreases. This is visualized in Fig. 1(a), where the configuration-averaged rates for the $1s^2 2p 20l$ states of O^{5+} ions obtained by the

AUTOSTRUCTURE [16] atomic structure code are shown. The full line is a fit to these points with the fit function being

$$A_a(n,l)=\tilde{A}_a n^{-3}\exp(\tilde{d}_1 l+\tilde{d}_2 l^2+\tilde{d}_3 l^3+\tilde{d}_4 l^4), \qquad (4)$$

and with the fit parameters $\tilde{A}_a$ and $\tilde{d}_i$.

Because of the neglect of type II transitions [cf. Eq. (1)] the radiative rate A_r is due only to the $2p\rightarrow 2s$ transition and therefore is independent of the Rydberg quantum numbers n and l. It is represented by the horizontal dashed line in Figs. 1(a) and 1(b).

In the limiting cases of $A_a \gg A_r$ or $A_r \gg A_a$ the cross section $\overline{\sigma}_{nl}^{(\mathrm{DR})}$ is given by

$$\overline{\sigma}_{nl}^{(\mathrm{DR})}=S_0\frac{g_d}{g_i}\frac{\pi}{E_n}A_<, \qquad (5)$$

where $A_<$ is the smaller of the rates A_a and A_r. For small values of l the autoionization rate A_a is far larger than the radiative rate A_r and the cross section $\overline{\sigma}_{nl}^{(\mathrm{DR})}$ is proportional to A_r. The autoionization rate decreases rapidly with increasing l and above a certain value l_c [vertical dotted line in Fig. 1(a)] it drops below the value of the radiative rate. Beyond that point the cross section $\overline{\sigma}_{nl}^{(\mathrm{DR})}$ is proportional to the autoionization rate A_a. However, this rate is so small that the contributions from states with l equal to l_c and above are negligible. This means that in this example where $l_c=10$ and the total number of states in the $1s^2 2p 20l$ manifold is 4800 the number of states participating in DR is reduced to $12l_c^2=1200$ with the resonance strength given by

$$\overline{\sigma}_{n}^{(\mathrm{DR})}\approx 6 l_c^2(n) S_0\frac{\pi}{E_n}A_<. \qquad (6)$$

The excluded states can be made available for DR by applying an electric field that mixes high-l states with lower-l states. More exactly, in the presence of an electric field the eigenstates of the ion are given by Stark states characterized by the quantum numbers n, κ, and m, and the DR cross section can be written as

$$\overline{\sigma}_{n}^{(DRF)}=(2j+1)S_0\frac{\pi}{E_n}\sum_{m\kappa}\frac{A_a(n,\kappa,m)A_r}{A_a(n,\kappa,m)+A_r}. \qquad (7)$$

In the case of full mixing the autoionization rates are simply given by

$$A_a(n,\kappa,m)=\sum_{l=|m|}^{n-1}(C_{\kappa,m}^{n,l})^2 A_a(n,l), \qquad (8)$$

with the Clebsch-Gordan coefficients [17]

$$C_{\kappa,m}^{n,l}=\left\langle \begin{matrix}(n-1)/2 & (n-1)/2\\ (m-\kappa)/2 & (m+\kappa)/2\end{matrix}\middle| \begin{matrix}l\\ m\end{matrix}\right\rangle \qquad (9)$$

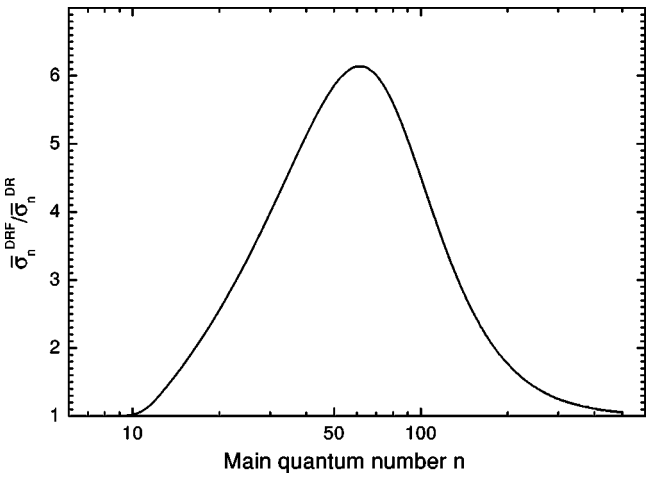

FIG. 2. Model calculation of the field-induced enhancement of the DR cross section of the $O^{4+}(1s^2 2pnl)$ resonances as a function of the main quantum number n.

for the transformation from spherical to Stark states. The sums over m and κ run over $-n+1,-n+2,\ldots,n-2,n-1$ and $-n+|m|+1,-n+|m|+3,\ldots,n+|m|-3,n-|m|-1$, respectively.

For the case of full mixing, the states significantly contributing to DR, i.e., the states for which the relation $A_a(n,\kappa,m)>A_r$ is valid, can be extracted from Fig. 1(b). The number of states is 1608, which is a factor of 1.34 higher than in the field-free case. The resulting enhancement is shown more quantitatively in Fig. 2 where the relation $\overline{\sigma}_n^{(DRF)}/\overline{\sigma}_n^{(\mathrm{DR})}$ is given as a function of n, and the cross section $\overline{\sigma}_n^{(\mathrm{DR})}$ has been calculated as $\overline{\sigma}_n^{(\mathrm{DR})}=\Sigma_l\overline{\sigma}_{nl}^{(\mathrm{DR})}$ with $\overline{\sigma}_{nl}^{(\mathrm{DR})}$ from Eq. (3). The field enhancement sets in at $n=10$, and then with increasing n reaches a maximum of $\overline{\sigma}_n^{(DRF)}/\overline{\sigma}_n^{(\mathrm{DR})}\approx 6$ at $n\approx 60$, and then it decreases again. Due to field ionization in the experiment, only Rydberg states up to $n\approx 29$ contribute significantly to the detected recombination rate (see below). That means only a small part of Rydberg states influenced by electromagnetic fields are detected.

In external electric fields m remains a good quantum number. This does not change if magnetic fields parallel to the electric fields are present in the interaction region [11]. However, in our experimental setup magnetic fields perpendicular to the applied electric fields are always present because of the longitudinal guiding field $B_\parallel$ in the electron cooler. This additional magnetic field mixes the m states, which further influences the recombination rate. At low magnetic fields m mixing in principle enhances the electric-field effect. At higher magnetic fields the rate enhancement decreases again, because of the increasing energy splitting of the m levels, which hampers the electric field mixing of these states [10,12]. In the theoretical treatment of DRF in crossed electric and magnetic fields the additional magnetic field requires the explicit consideration of each m substate, increasing the computational demand significantly. Calculations of DR in crossed electric and magnetic fields can therefore presently only be carried out for relatively low values of n, i.e., $n\lesssim 30$. For a detailed comparison of experiment and theory,

the observation of DRF on a single low-n resonance would be required. In the experiment, however, low-n resonances that can be resolved are not affected by external fields and high-n resonances that are affected cannot be resolved. Therefore, an adaption of the method used for Mg^+ [4,5] is introduced to investigate DRF for narrow-bandwidth samples of n states. This approach employs state selective field ionization of high-n Rydberg states.

III. THEORY

The DR calculations in the absence of fields have been carried out using the atomic structure code AUTOSTRUCTURE [16]. For the DRF calculations the program DRFEUD (dielectronic recombination field enhanced using diagonalization) [18] has been used. This calculates the intermediate coupled, energy averaged DR cross section for a given field in the interaction region. It was first developed to calculate the influence of a pure electric field on DR. The wave functions are solutions to the Hartree-Fock equations with relativistic modifications. Since diagonalization of the Hamiltonian matrices has to be performed for each value of n and m, the program had to be designed for efficiency. The number of matrices that have to be solved is reduced by the fact that the cross section falls off rather rapidly with m and matrices for high m can be excluded. This changes as a magnetic field perpendicular to the electric field is introduced [12] and m is no longer a good quantum number. The Hamiltonian matrix then becomes extremely large leading to computational problems. In Ref. [12] an upper limit of $n=30$ set by available computer memory is mentioned. However, for low Z ions the cutoff value n_c is in the same range, so that calculations on DR in crossed electric and magnetic fields can be carried out for nearly all states involved experimentally.

These calculations do not account for the effect of interacting resonances, which was treated by Robicheaux *et al.* [19] and Griffin *et al.* [20]. They modified the DRFEUD program to include interacting resonances in the calculation of DR in electric fields. However, the Hamiltonian then becomes complex; thus such calculations were not carried out in the presence of crossed electric and magnetic fields, since the complex matrices become prohibitively large.

The electric field in the interaction region defines a quantization axis. Before being detected, the ions in high Rydberg states pass through motional electric fields that are rotated with respect to this axis, which could lead to a redistribution of m substate populations. This effect has been theoretically treated by Nasser and Hahn [21]. A comparison of their theoretical data to experimental results of Müller *et al.* [4] showed that these effects should be considered in general. However, in our experiments, these effects do not appear to be important, as has been shown by Schippers *et al.* [15].

IV. EXPERIMENT

The experiment has been carried out at the heavy-ion storage ring CRYRING at the Manne Siegbahn Laboratory in Stockholm. The experimental procedure for DRF measurements at CRYRING is explained in more detail in Ref. [13].

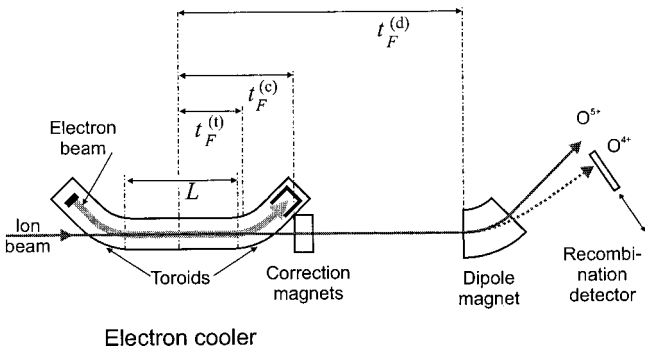

FIG. 3. Schematic representation of the experimental setup. The ion beam enters the electron cooler from the left. There it is merged with a cold electron beam. On their way from the merging section to the detector the recombined ions pass several regions where they can possibly be field ionized in motional electric fields. The flight time to these field-ionization regions are indicated.

Here only an outline is given. The $^{16}O^{5+}$ ions were produced in a cryogenic electron-beam ion source (CRYSIS), preaccelerated by a radio frequency quadrupole to about 300 keV/u, injected into the ring, and accelerated to their final energy. The ion energies used in our experiment were 9.4 MeV/u (which is almost the highest energy that can be achieved at CRYRING), 5.0 MeV/u, and 3.3 MeV/u. A further lowering of the ion energy was not possible because of strongly increasing background of electron capture events arising from collisions of ions with the residual gas. The ion beam has a large energy spread and therefore has to be cooled. This is done with a colinear beam of cold electrons in an electron cooler [22] as illustrated in Fig. 3. The cooler consists of three main parts that are the cathode, the interaction region, and the collector. Each of these parts is surrounded by a magnet. Two toroid magnets are used to deflect the electron beam into the interaction region and out into the collector. The vertical component of the magnetic field in the toroid magnets causes a horizontal deflection of the ion beam that is compensated by a correction dipole magnet placed just behind the cooler. The 4 mm cathode for electrons is immersed in a 3 T magnetic field. The emitted electron beam has an energy spread determined essentially by the cathode temperature $T_c \approx 900\,^\circ$ C. The longitudinal energy spread of the electron beam is reduced by the electrostatic acceleration of the electrons. The transverse energy spread is reduced as the electron beam expands in the decreasing axial magnetic field [23]. After expansion the transverse electron beam temperature amounts to

$$T_\perp = \frac{1}{\zeta} T_c , \tag{10}$$

with the expansion factor $\zeta = B_\parallel^c / B_\parallel = 29.6$ calculated from the magnetic guiding field $B_\parallel^c$ at the cathode and $B_\parallel = 100.6$ mT in the straight section of the electron cooler. After expansion and acceleration the electron velocity distribution $f(\hat{v},\vec{v})$ around the average parallel velocity component $\hat{v}$ can be described as

$$f(\hat{v},\vec{v}) = \sqrt{\frac{m_e}{2\pi k_B T_\parallel}} \exp\left[-\frac{m_e (v_\parallel - \hat{v})^2}{2 k_B T_\parallel} \right] \frac{m_e}{2\pi k_B T_\perp} \times \exp\left(-\frac{m_e v_\perp^2}{2 k_B T_\perp} \right), \tag{11}$$

with $kT_\parallel = 0.35$ meV and $kT_\perp = 3.7$ meV in the present case. The experimental energy resolution corresponds to the width of this distribution and amounts to [24]

$$\Delta\hat{E}(\mathrm{FWHM}) = \{[\ln(2) k_B T_\perp]^2 + 16 \ln(2) k_B T_\parallel \hat{E}\}^{1/2}. \tag{12}$$

The relative energy $\hat{E} \approx 1/2 m_e \hat{v}^2$ was calculated more accurately using the relativistic transformation of energies from the laboratory to the center-of-mass frame including the angle between the beams. In the course of our DRF measurements, this angle acquired values up to about 1°. To verify the energy scale we used the Rydberg formula [Eq. (2)], neglecting quantum defects, to fit the measured resonance energies. Spectroscopic values were used for the $E_{2s\rightarrow 2p}$ transition.

The absolute merged-beams rate coefficient is given by [25]:

$$\alpha = \langle v\, \sigma(v) \rangle = \frac{R v_i q e}{I_i L n_e} \gamma_i^2 . \tag{13}$$

Here R is the count rate, v_i the ion velocity, q the ion charge, e the elementary charge, γ_i the Lorentz factor for the ions, I_i the ion current, L the interaction length (95 cm), and n_e the electron density that is assumed to be constant across the diameter of the electron beam.

After injecting ions into the ring, accelerating and cooling them, the relative-energy range $0 < \hat{E} < 15$ eV was scanned by varying the cathode voltage. This was done five times for different electric fields with 1 s of intermediate cooling. The remaining ions were then dumped and the whole cycle started over. This was repeated until a satisfactory level of statistical precision was reached.

Electric fields were introduced in the interaction region by employing correction coils mounted on top of the solenoid that produces the longitudinal guiding field $B_\parallel$. The correction coils usually serve for optimizing the alignment of the electron beam with respect to the ion beam. In the present experiments, these coils are used to introduce well defined transverse magnetic-field components $B_\perp$, which transform to electric fields $E_\perp = v_i B_\perp$ in the rest frame of an ion. In order to avoid confusion it should be noted that the motional electric field $E_\perp$ in the interaction region, that causes the enhancement of the DR cross section is different and spatially well separated from the motional electric fields F that cause field ionization of recombined ions in high Rydberg states as will be discussed in Sec. IV A.

The uncertainty of the determination of the ion current with the current transformer is about $\pm 10\%$ and the uncertainty of the interaction length is about $\pm 5\%$. The ion current was only measured for one spectrum at the beginning of the run and all other spectra were normalized to that one. The relative ion current for the spectra in one cycle was determined by a fit to the radiative recombination rate observed during the intermediate cooling intervals. The uncertainty for that is about 1%. The statistical uncertainty for the integrated recombination rate is also about 1%. Background subtraction (here radiative recombination is regarded as background) was achieved by fitting a formula with five fit parameters P_i,

$$\alpha_b(E) = \frac{P_1}{1 + P_2 E + P_3 E^2} + P_4 + P_5 E \tag{14}$$

to those parts of the measured spectra where no DR resonances occurred. All uncertainties added in quadrature including those for background subtraction add up to 11% uncertainty in the absolute rate coefficients.

A. Field ionization

In view of the determination of DR rate coefficients differential in the Rydberg quantum number n of the $O^{4+}(1s^2 2pnl)$ DR resonances, the field ionizing properties of our experimental setup have to be known. In the following, a detailed model is described, which accounts for the field ionization of high Rydberg states in motional electric fields caused by the magnetic fields that are used to steer the electron and ion beams. Furthermore, the model accounts for the radiative decay of high Rydberg states to levels below the field-ionization limit. The model was introduced by Schippers *et al.* [26] for analyzing recombination measurements at the heavy-ion storage ring TSR and is here modified for the CRYRING experiments.

On their way from the interaction region to the detector the ions pass through three magnets. These are (i) the toroid magnet that guides the electron beam out of overlap, (ii) the correction dipole magnet just after the cooler, and (iii) the bending dipole magnet that separates the different charge states (Fig. 3). The transverse magnetic fields that these magnets exert on the ions cause electric fields $\vec{F} = \vec{v}_i \times \vec{B}$ in the system of the ions. The fields are listed in Table I and their variation along the path of the ions is shown in Fig. 4. These fields ionize ions in highly excited Rydberg states. In a simplified treatment only recombined ions with the electron captured into states $n < n_c$ account for the measured recombination rate. Considering the Stark shifts in the lowest order in F, n_c can be approximately calculated as

$$n_c = [q^3/9F]^{1/4}, \tag{15}$$

where F is the electric field in atomic units (1 au $= 5.142 \times 10^9$ V/cm) [27]. In the detailed model of the field-ionization properties of our apparatus, the survival fractions are determined for each nl state populated by DR, considering the flight times t_F to the field-ionization zones and assuming hydrogenic decay rates of the Rydberg states. With a constant recombination probability along the length L of the merging section, the probability that a state characterized by quantum numbers n and l has decayed upon reaching the field ionization zone is given as [26]

TABLE I. The motional electric fields F leading to field ionization are given for the different magnets passed by the recombined ions on their way to the detector, the toroid, the correction dipole magnet, and the ring dipole magnet. t_F is the flight time to the corresponding field, Δt_F the dwell time in this field, and n_c is the critical quantum number for field ionization.

E_i (MeV/u)	Region	F (kV/cm)	Δt_F (ns)	t_F (ns)	n_c
	Toroid	21	9. 2	19	42
9.4	Correction magnet	60	5	14	33
	Dipole magnet	490	27	11	19
	Toroid	16	12	25	46
5. 0	Correction magnet	45	6. 6	19	35
	Dipole magnet	276	36	15	22
	Toroid	13	15	31	48
3. 3	Correction magnet	36	8	23	37
	Dipole magnet	177	45	19	25

$$P_d(n,l,t_L,t_F)=1-\frac{\tau(n,l)}{t_L}\left[\exp\left(-\frac{t_F-t_L/2}{\tau(n,l)}\right)-\exp\left(-\frac{t_F+t_L/2}{\tau(n,l)}\right)\right]. \quad (16)$$

Here t_L is the flight time through the electron cooler, t_F is the flight time from the center of the cooler to the field-ionization zone, and the radiative lifetime of the nl state is given by $\tau(nl)=[\Sigma_{n'<n,\,l'=l\pm1}\gamma_r(nl\rightarrow n'l')]^{-1}$. The hydrogenic transition rates $\gamma_r(nl\rightarrow n'l')$ are calculated analyticaly [28]. In the field-ionization zone the ion spends a time Δt_F during which field ionization may take place. As in Ref. [5], the ion's survival probability is calculated from approximate hydrogenic field-ionization rates A_F derived by Damburg and Kolosov [29] (modified in order to account for an arbitrary nuclear charge [26]) to be

$$P_s(n,l,\Delta t_F,F)=\frac{1}{2l+1}\sum_{m=-l}^{l}\sum_{n_1=0}^{n-|m|-1}(C^{n,l}_{\kappa,m})^2\times\exp[-\Delta t_F A_F(n_1,n_2,m)], \quad (17)$$

where $C^{n,l}_{\kappa,m}$ are the Clebsch-Gordan coefficients from Eq. (9) and n_1 and n_2 are the parabolic quantum numbers, which satisfy the relations $n=n_1+n_2+|m|+1$ and $n_1-n_2=\kappa$ [27]. The detection probability is calculated from the decay and survival probabilities as [26]

$$\Upsilon_{nl}(t_L,t_F,\Delta t_F,F)=[1-P_d(n,l,t_L,t_F)]\,P_s(n,l,\Delta t_F,F)+\sum_{n'<n,\,l'=l\pm1}b(nl\rightarrow n'l')\times P_d(n,l,t_L,t_F)P_s(n',l',\Delta t_F,F), \quad (18)$$

where the branching ratio for a dipole transition from state nl to state $n'l'$ is defined as $b(nl\rightarrow n'l')=\tau(n,l)\,\gamma_r(nl\rightarrow n'l')$. A more general formula including cascade correction can be found in Ref. [26]. Here, cascading has been neglected because transitions to lower n' always dominate as has been verified for DR of C^{3+} [26]. High l states where cascading would be important are not significantly populated by DR. To obtain the detection probability, we have to consider all field-ionization regions shown in Fig. 4. The corresponding detection probabilities $\Upsilon^{(t)}_{nl}$, $\Upsilon^{(c)}_{nl}$, and $\Upsilon^{(d)}_{nl}$, respectively, are calculated individually and the overall detection probability is finally given by the product of the three individual ones, i.e.,

$$\Upsilon_{nl}(v_i)=\Upsilon^{(t)}_{nl}(t^{(t)}_F,\Delta t^{(t)}_F,F^{(t)})\Upsilon^{(c)}_{nl}(t^{(c)}_F-t^{(t)}_F,\Delta t^{(c)}_F,F^{(c)})\times\Upsilon^{(d)}_{nl}(t^{(d)}_F-t^{(c)}_F,\Delta t^{(d)}_F,F^{(d)}). \quad (19)$$

For the calculation of $\Upsilon^{(c)}_{nl}$ and $\Upsilon^{(d)}_{nl}$ the $t_L\rightarrow0$ limit of Eq. (16), i.e., $P_d(n,l,0,t_F)=1-\exp[-t_F/\tau(n,l)]$ has been used. The dependence on the ion velocity enters via the v_i dependence of t_F, Δt_F, and F. Numerical values of t_F, Δt_F, and F for the three experimental ion velocities are listed in Table I. Detection probabilities for 3.3 MeV/u ions are shown in Fig. 5. In contrast to the simple concept of a sharp cutoff at n_c [Eq. (15)] a considerable fraction of low-l Rydberg states is detected with high probability even for high n, i.e., $n\gg n_c$.

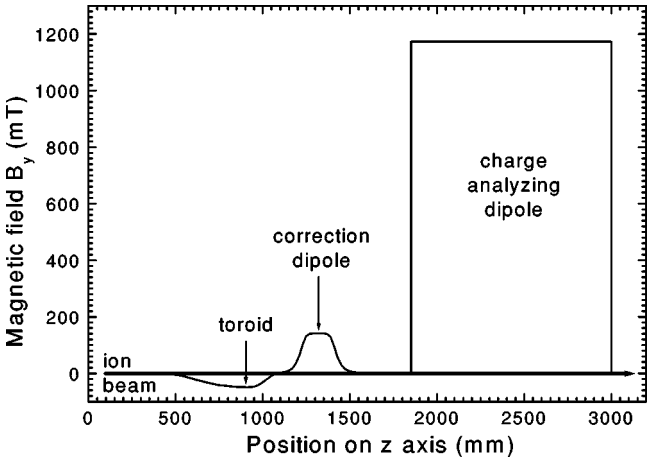

FIG. 4. Magnetic fields encountered by the ion beam on its way from the cooler to the recombination detector. In the frame of the ion the magnetic fields transform into electric fields leading to field ionization of high Rydberg states. The values for the toroid and the correction dipole magnet have been measured. For completeness, the magnetic field of the bending dipole magnet has been added schematically.

V. RESULTS AND DISCUSSION

A. Field-free DR

For three different ion energies recombination spectra have been obtained for a set of different electric fields $E_\perp$. The field-free spectrum ($E_\perp=0$ V/cm) for an ion energy of 9.4 MeV/u is shown in Fig. 6(a). It contains all $1s^22pnl$ resonances associated with $2s\rightarrow2p$ transitions ranging from $n=6$, which is the lowest energetically allowed resonance,

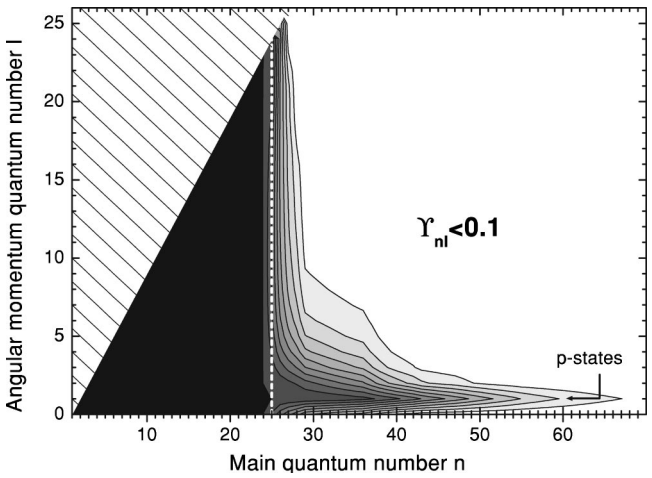

FIG. 5. Contour plot of detection probabilities $\Upsilon_{nl}(v_i)$ for an ion energy of 3. 3 MeV/u from the detailed model described in Sec. IV A. Each contour line marks a step of 0.1 in the detection probability. A considerable fraction of low-l Rydberg states is detected with high probability even for high $n>n_c$. The vertical white broken line is the cutoff quantum number $n_c=25$ as calculated by Eq. (15). The hatched area is unphysical.

up to $n\approx 20$. Individual resonances can be resolved up to $n=15$. For $n=6$, even the l substates are partially resolved. Figure 6(b) shows an AUTOSTRUCTURE calculation that does not include field ionization. The highest Rydberg state considered is $n=1000$.

The access to DR differential in n is via the unavoidable field ionization described in Sec. IV A. It limits the maximum detected Rydberg state roughly to n_c [Eq. (15), Table I]. The motional electric field F depends on the ion velocity, i.e.,

$$F=\frac{\gamma_i m_i v_i^2}{qe\rho}. \tag{20}$$

As the ion velocity is decreased, the magnetic field of the bending dipole magnets (with bending radius ρ) is reduced and therewith the motional electric field $F=v_iB$. This shifts the cutoff quantum number n_c to higher values. The field-free spectra for all three energies are shown in Fig. 7 together with results from an AUTOSTRUCTURE calculation to which the field-ionization model has been applied by multiplying the nl-dependent DR cross section with the nl-dependent survival probability. For the comparison the theoretical cross section has been convoluted with the experimental velocity distribution resulting in the theoretical rate coefficient

$$\alpha(\hat{E})=\sum_{nl}\ \Upsilon_{nl}(v_i)\int \sigma_{nl}(E(v))v\ f(\hat{v},\vec{v})d^3v. \tag{21}$$

Since the natural width of the DR resonances is negligible compared to the experimental energy spread, we assume a δ-like energy dependence of the DR cross section, i.e.,

$$\sigma_{nl}(E)=\overline{\sigma}_{nl}\delta(E_n-E) \tag{22}$$

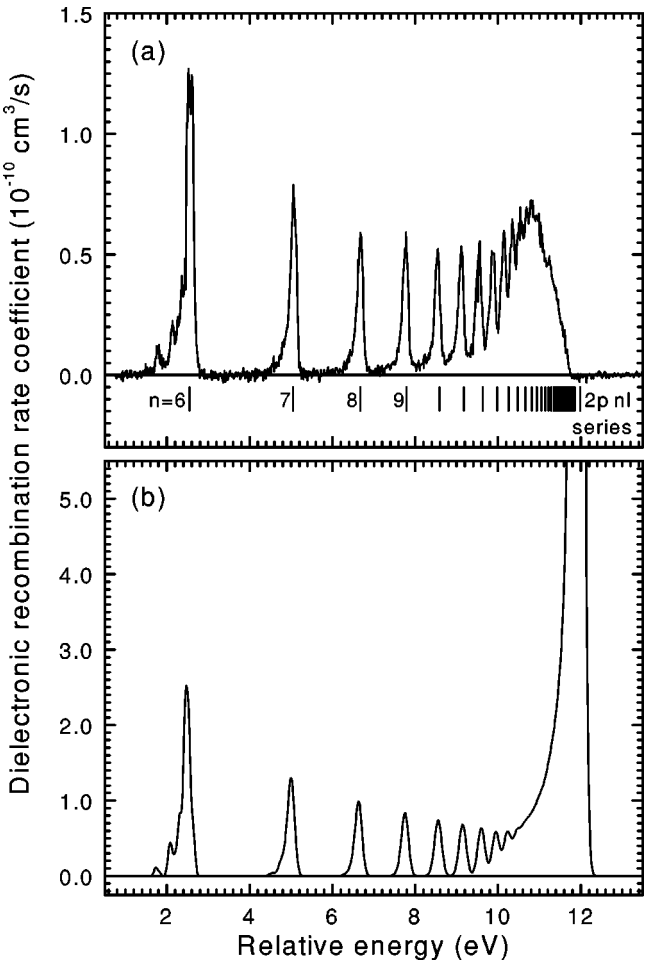

FIG. 6. (a) Zero-field O^{5+} DR spectrum for an ion energy of 9.4 MeV/u. (b) The AUTOSTRUCTURE calculation including Rydberg states up to $n=1000$ demonstrates that due to field ionization most of the recombination rate contributed by high Rydberg states is not detected in the experiment. The vertical bars denote the $2pnl$ resonance positions as calculated by the Rydberg formula [Eq. (2)].

with the resonance energy E_n. Under this condition the integration in Eq. (21) can be carried out analytically and we obtain

$$\alpha^{(\mathrm{DR})}(\hat{E})=\sum_{nl}\ \sqrt{\frac{2E_n}{m_e}}\Upsilon_{nl}(v_i)\overline{\sigma}_{nl}^{(\mathrm{DR})}f(\hat{E},E_n), \tag{23}$$

where

$$f(\hat{E},E)=\frac{1}{k_BT_\perp\xi}\exp\left(-\frac{E-\hat{E}/\xi^2}{k_BT_\perp}\right)\left[\mathrm{erf}\left(\frac{\sqrt{E}+\sqrt{\hat{E}}/\xi^2}{\sqrt{k_BT_\parallel}/\xi}\right)+\mathrm{erf}\left(\frac{\sqrt{E}-\sqrt{\hat{E}}/\xi^2}{\sqrt{k_BT_\parallel}/\xi}\right)\right], \tag{24}$$

with $\xi=(1-T_\parallel/T_\perp)^{1/2}$. As the ion energy is decreased and n_c grows, the recombination rate coefficient in the high-energy part of the spectra increases. Experimental and theo-

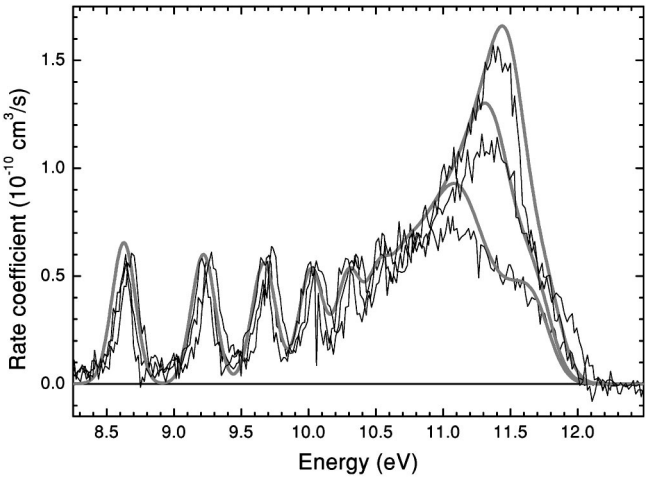

FIG. 7. Zero-field O^{5+} DR spectra for three different ion energies 9.4, 5.0, and 3.3 MeV/u. With decreasing ion energy, increasingly higher Rydberg states contribute to the measured rate coefficient. Included are the theoretical results to which our field-ionization model has been applied (thick gray lines).

retical data shown in Fig. 7 agree quite nicely. From this we conclude that field ionization is sufficiently well understood in our experiment.

B. DRF

For each ion energy a series of spectra were taken for different applied electric fields $E_\perp$. The ranges of electric fields are listed in Table II. With decreasing ion velocity the maximum electric field ($E_\perp = v_i B_\perp$) decreases. The longitudinal guiding field was 100.6 mT for all measurements.

The enhancement of the DR via high Rydberg states is quantified by extracting rate coefficients $I_{\rm hi}$ integrated over the energy range of 9.4–12 eV of the measured spectra (Fig. 8). For normalization purposes we also monitored the integral $I_{\rm lo}$ (1.3–7.25 eV) comprising DR contributions from $n = 6$–8. The high Rydberg contributions $I_{\rm hi}$ monotonically increase with the electric field, while the lower-n contribution $I_{\rm lo}$ remains constant when the electric field is changed. In order to provide a quantity characterizing the field effects we use the electric-field enhancement factor [14]

$$r(E_y) = C \frac{I_{\rm hi}(E_y)}{I_{\rm lo}(E_y)}. \tag{25}$$

The constant C is conventionally chosen such that fits to the data points (see below) yield $r^{(\rm fit)}(0) = 1.0$. The formula

TABLE II. Ranges of motional electric fields $E_\perp = v_i B_\perp$ that were applied in the experiment. Here v_i is the ion velocity and $B_\perp$ the transverse magnetic field. The values are given for the three experimental ion energies.

E_i (MeV/u)	v_i (10^9 cm/s)	$B_\perp$ (mT)	E (V/cm)
9. 4	4. 20	0–1.4	0–602
5. 0	3. 15	0–1.4	0–449
3. 3	2. 53	0–1.2	0–301

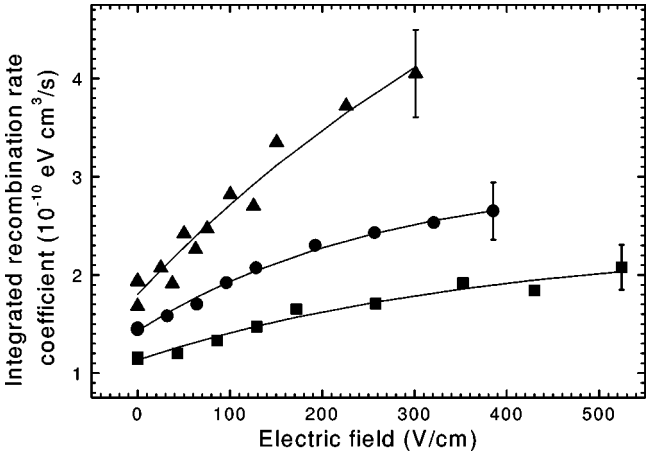

FIG. 8. Integrals $I_{\rm hi}$ from 9.4 to 12 eV for all three ion energies 9.4 MeV/u (squares), 5.0 MeV/u (circles), and 3.3 MeV/u (triangles). The curves were fitted using Eq. (26). The error bars represent the normalization error of 11% given in Sec. IV.

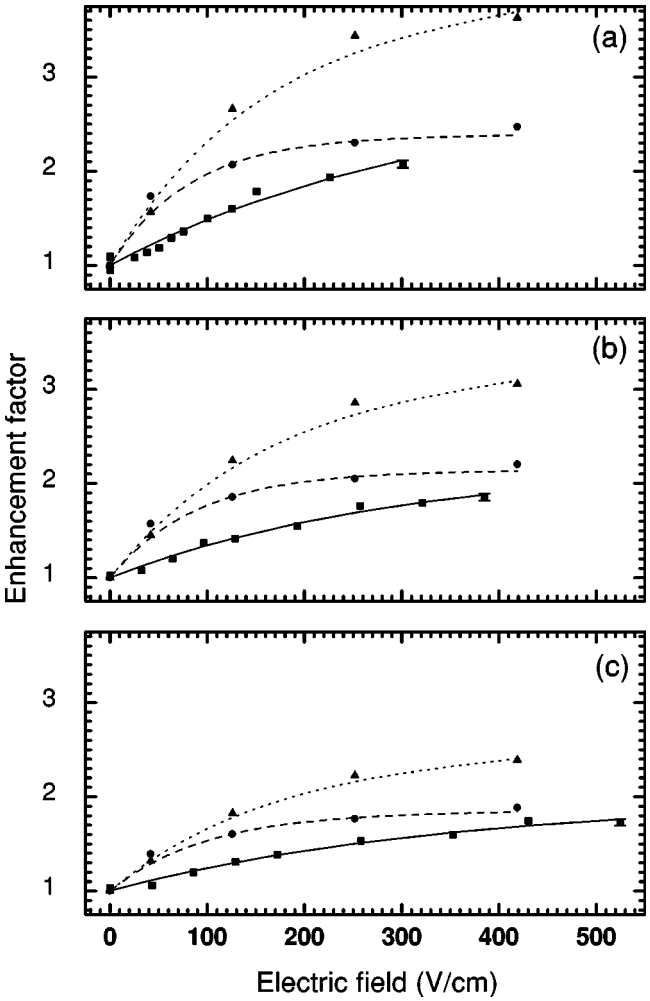

FIG. 9. Enhancement of the recombination rate due to an electric field for 9.4 MeV/u (c), 5.0 MeV/u (b), and 3.3 MeV/u (a). Each panel includes the experimental result (squares, full line), the theoretical result with $B_\parallel = 0$ T (circles, dashed line), and the theoretical result for $B_\parallel = 100.6$ mT (triangles, dotted line). The curves have been fitted to the data points using Eq. (26). The fit values s and $E_{\rm sat}$ are given in Table III.

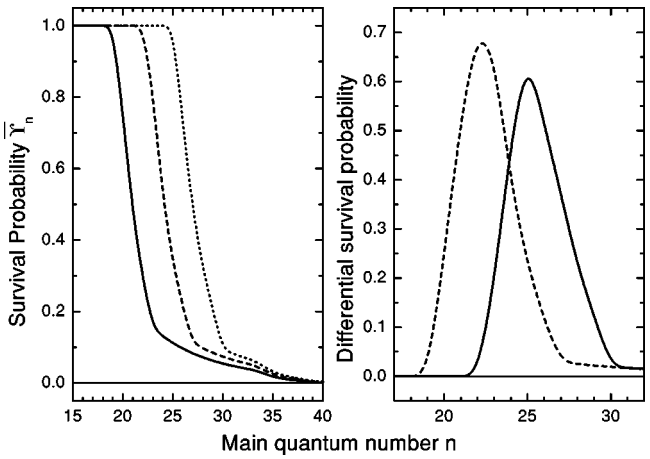

FIG. 10. (a) Survival probabilities $\overline{Y}_n(v_i)$ averaged over the angular momentum for the three experimental ion energies 9.4, 5.0, and 3.3 MeV/u (from left to right) (b) Differential survival probabilities, i.e., the difference between adjacent curves shown in (a).

$$r^{(\mathrm{fit})}(E_y)=1+sE_{\mathrm{sat}}[1-\exp(-E_y/E_{\mathrm{sat}})], \qquad (26)$$

which we have fitted to the measured enhancement factors, provides an easy parametrization of our data. The parameter E_{sat} is the saturation field and s is the initial slope, which is the tangent to $r^{(\mathrm{fit})}(E_y)$ at $E_y=0$. The result of the present experiment is shown in Fig. 9. The enhancement factor first grows linearly and then saturates for high electric fields. For these high fields the maximum mixture of l states is achieved. This saturation has been seen even more clearly in our Ne^{7+} experiment [13]. For decreasing ion energy, the enhancement of the recombination rate increases. This is due to the fact that the additional higher n states are more sensitive to electromagnetic fields (as shown in Fig. 2).

Curves have been fitted to the data shown in Fig. 8 using Eq. (26). The difference between these curves is associated with n states added by lowering the ion energy [$n\approx 20$–26 and $n\approx 23$–29 as shown in Fig. 10(a)]. By subtracting the curves from one another one gets the integrated recombination rate coefficient only due to these two n bands. After obtaining the integrated recombination-rate coefficient for these two n bands one can determine the enhancement factors for these samples as described above.

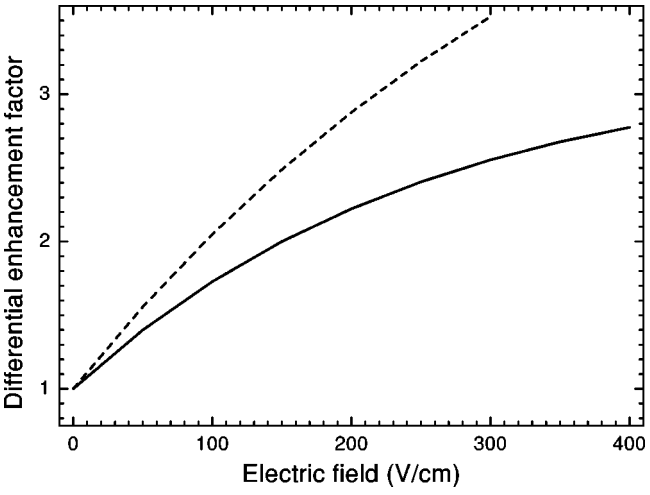

FIG. 11. The enhancement of the recombination rate of the two distributions of n states shown in Fig. 10(b) (solid line, $n=20$–26, dashed line, $n=23$–29).

TABLE III. Parameters of the fit [Eq. (26)] to the measured and the theoretical data of the enhancement factor. Here s is the initial slope and E_{sat} is the saturation field.

	E_i (MeV/u)	s (10^{-3} cm/V)	E_{sat} (V/cm)
Experiment	9.4	2.8 ± 0.22	354 ± 61.1
($B_{\parallel}=100.6$ mT)	5.0	4.0 ± 0.30	304 ± 56.0
	3.3	5.6 ± 0.53	347 ± 118
Theory	9.4	9.8 ± 1.6	86 ± 18
($B_{\parallel}=0$ mT)	5.0	15 ± 2.6	75 ± 15
	3.3	20 ± 3.6	68 ± 14
Theory	9.4	9.4 ± 0.4	161 ± 9.8
($B_{\parallel}=100.6$ mT)	5.0	14 ± 1.0	159 ± 17
	3.3	19 ± 1.8	149 ± 21

The result is shown in Fig. 11. The enhancement factor at 300 V/cm increases from 2.5 for $n=20$–26 to 3.5 for $n=23$–29, i.e., the sensitivity to electromagnetic fields increases for growing n as suggested by the model calculation (see Fig. 2).

In the comparison of theoretical and experimental results the following problem has to be considered. In the presence of an electric field alone or crossed electric and magnetic fields, the angular momentum l is not a good quantum number. On the other hand, in order to compare these results to our experimental data we have to use our field-ionization model that calculates nl dependent detection probabilities. In a proper treatment the l and m mixed states in the interaction region would have to be mapped onto spherical states when the ion leaves the cooler. Such a mapping, however, is pres-

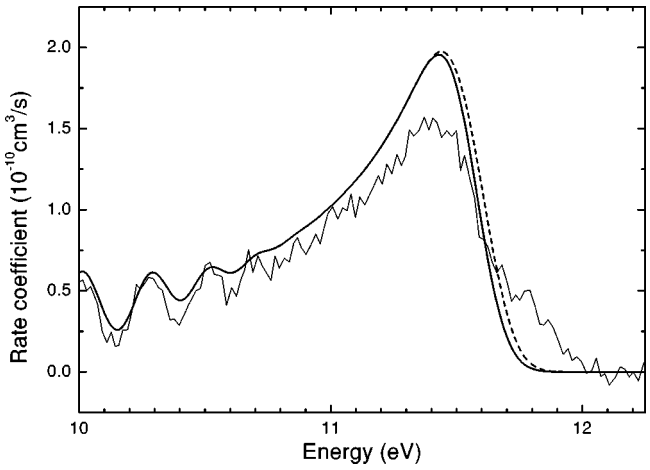

FIG. 12. Experimental DR spectra for an ion energy of 3.3 MeV/u (full line) and an AUTOSTRUCTURE calculation up to $n=30$ to which the field-ionization model has been applied using nl dependent detection probabilities (thick dashed line) and l-averaged detection probabilities (thick full line).

ently not at hand since the theoretical data can only be given as a function of n. Therefore we use l averaged detection probabilities,

$$\overline{\Upsilon}_n(v_i)=\frac{1}{n^2}\sum_{l=0}^{n-1}(2l+1)\Upsilon_{nl}(v_i). \tag{27}$$

The difference in using nl dependent and l averaged detection probabilities is small as shown in Fig. 12 where both have been applied to a zero field AUTOSTRUCTURE calculation. DRF has been calculated using the DRFEUD package. This has been done for 0, 42, 126, 252, and 419 V/cm for the case of a pure electric field in the interaction region and for a magnetic field of 100.6 mT. From the theoretical cross section we have derived a rate coefficient analog to Eq. (23), i.e.,

$$\alpha(\hat{E})^{(DRF)}=\sum_n \overline{\Upsilon}_n(v_i)\overline{\sigma}_n^{(DRF)}f(\hat{E},E_n). \tag{28}$$

In the next step theoretical integrals $I_{\rm hi}$ from 9.4–12 eV have been derived, which were used to obtain theoretical enhancement factors included in Fig. 9. This has been done for all three ion energies. The theoretical result is far above the experimental result for the whole range of electric fields. A reason for part of this discrepancy could be the fact that these calculations have been carried out in the isolated resonances approximation. It has been shown by Robicheaux *et al.* [19] and Griffin *et al.* [20] that the static field enhancement of DR may be strongly reduced by the interaction between resonances through common continua. Because of the size of the complex matrices involved, the investigation of these effects in lithiumlike ions for crossed electric and magnetic fields is not yet possible.

VI. SUMMARY AND CONCLUSIONS

Previous studies of dielectronic recombination in the presence of electromagnetic fields have been extended towards elements with lower atomic number Z where in our storage ring merged-beam experiments field ionization sets in much earlier than for higher Z values. Nevertheless, still an enhancement up to a factor of 2 can be observed. A first step has been made to provide n-differential DRF data. This has been done by varying the ion energy. The additional narrow-bandwidth sets of detected Rydberg states has been determined using a field-ionization model. Comparing the influence of electromagnetic fields on the two sets ($n=20$–26 and $n=23$–29) an increasing sensitivity to these fields has been observed. Comparison of the field-free experimental data to theory after applying the field-ionization model described in Sec. IV shows a quite good agreement, especially for high n states.

The experimental results on DR in fields are compared to theoretical calculations. The theoretically calculated enhancement is about 50% above the experimental result, i.e., the experimental DRF measurements cannot quantitatively be explained by state-of-the-art theory. Based on previous theoretical results for DRF in zero magnetic field [19,20] it can be speculated that the effect of interacting resonances has to be considered also for DR in crossed electric and magnetic fields in order to remove the remaining discrepancies. On the experimental side it is difficult to judge how far the approximation in the field-ionization modeling affects the comparison with theory. Further experimental and theoretical efforts are clearly needed for a full understanding of the DRF process.

ACKNOWLEDGMENTS

We gratefully acknowledge support by Deutsche Forschungsgemeinschaft under Project No. MU 1068/8. We thank G. H. Dunn for his suggestions concerning the manuscript. D.M.M. and D.C.G. were supported by the U.S. Department of Energy, Grant No. DE-FG02-96-ER54367 with Rollins College.

[1] A. Burgess and H.P. Summers, Astrophys. J. **157**, 1007 (1969).
[2] V.L. Jacobs, J. Davis, and P.C. Kepple, Phys. Rev. Lett. **37**, 1390 (1976).
[3] V.L. Jacobs and J. Davis, Phys. Rev. A **19**, 776 (1979).
[4] A. Müller, D.S. Belić, B.D. DePaola, N. Djurić, G.H. Dunn, D.W. Mueller, and C. Timmer, Phys. Rev. Lett. **56**, 127 (1986).
[5] A. Müller, D.S. Belić, B.D. DePaola, N. Djurić, G.H. Dunn, D.W. Mueller, and C. Timmer, Phys. Rev. A **36**, 599 (1987).
[6] K. LaGattuta, I. Nasser, and Y. Hahn, Phys. Rev. A **33**, 2782 (1986).
[7] C. Bottcher, D.C. Griffin, and M.S. Pindzola, Phys. Rev. A **34**, 860 (1986).
[8] T. Bartsch, A. Müller, W. Spies, J. Linkemann, H. Danared, D.R. DeWitt, H. Gao, W. Zong, R. Schuch, A. Wolf, G.H. Dunn, M.S. Pindzola, and D.C. Griffin, Phys. Rev. Lett. **79**, 2233 (1997).
[9] F. Robicheaux and M.S. Pindzola, Phys. Rev. Lett. **79**, 2237 (1997).
[10] T. Bartsch, S. Schippers, A. Müller, C. Brandau, G. Gwinner, A.A. Saghiri, M. Beutelspacher, M. Grieser, D. Schwalm, A. Wolf, H. Danared, and G.H. Dunn, Phys. Rev. Lett. **82**, 3779 (1999).
[11] V. Klimenko, L. Ko, and T.F. Gallagher, Phys. Rev. Lett. **83**, 3808 (1999).
[12] D.C. Griffin, F. Robicheaux, and M.S. Pindzola, Phys. Rev. A **57**, 2708 (1998).
[13] S. Böhm, S. Schippers, W. Shi, A. Müller, N. Djurić, G.H. Dunn, W. Zong, B. Jelencović, N. Eklöw, P. Glans, R. Schuch, and H. Danared, Phys. Rev. A **64**, 032707 (2001).
[14] T. Bartsch, S. Schippers, M. Beutelspacher, S. Böhm, M. Grieser, G. Gwinner, A.A. Saghiri, G. Saathoff, R. Schuch, D. Schwalm, A. Wolf, and A. Müller, J. Phys. B **33**, L453 (2000).

[15] S. Schippers, T. Bartsch, C. Brandau, A. Müller, G. Gwinner, G. Wissler, M. Beutelspacher, M. Grieser, A. Wolf, and R.A. Phaneuf, Phys. Rev. A **62**, 022708 (2000).
[16] N.R. Badnell, J. Phys. B **19**, 3827 (1986).
[17] D. Park, Z. Phys. **159**, 155 (1960).
[18] D.C. Griffin, M.S. Pindzola, and C. Bottcher, Phys. Rev. A **33**, 3124 (1986).
[19] F. Robicheaux, M.S. Pindzola, and D.C. Griffin, Phys. Rev. Lett. **80**, 1402 (1998).
[20] D.C. Griffin, D. Mitnik, M.S. Pindzola, and F. Robicheaux, Phys. Rev. A **58**, 4548 (1998).
[21] I. Nasser and Y. Hahn, Phys. Rev. A **36**, 4704 (1987).
[22] H. Danared, A. Källberg, G. Andler, L. Bagge, F. Österdahl, A. Paál, K.G. Rensfelt, A. Simonsson, Ö. Skeppstedt, and M. af Ugglas, Nucl. Instrum. Methods Phys. Res. A **441**, 123 (2000).
[23] H. Danared, G. Andler, L. Bagge, C.J. Herrlander, J. Hilke, J. Jeansson, A. Källberg, A. Nilsson, A. Paál, K.G. Rensfelt, U. Rosengård, J. Starker, and M. af Ugglas, Phys. Rev. Lett. **72**, 3775 (1994).
[24] A. Müller, Int. J. Mass. Spectrom. **192**, 9 (1999).
[25] G. Kilgus, D. Habs, D. Schwalm, A. Wolf, N.R. Badnell, and A. Müller, Phys. Rev. A **46**, 5730 (1992).
[26] S. Schippers, A. Müller, G. Gwinner, J. Linkemann, A.A. Saghiri, and A. Wolf, Astrophys. J. **555**, 1027 (2001).
[27] T.F. Gallagher, *Rydberg Atoms* (Cambridge University, Cambridge, England, 1994).
[28] H.A. Bethe and E.E. Salpeter, *Quantum Mechanics of One- and Two-Electron Atoms* (Plenum, New York, 1977).
[29] R.J. Damburg and V.V. Kolosov, J. Phys. B **12**, 2637 (1979).